THE TOPOGRAPHY OF EPIMETHEUS

PHILIP J. STOOKE

Department of Geography, University of Western Ontario, London, Ontario, Canada

Abstract. A topographic model of Saturn's smaller co-orbital satellite Epimetheus was derived from the shapes of limbs, terminators and shadows of the F Ring in Voyager images, modified locally to accommodate large craters and ridges. The model is presented here in tabular and graphic form, including the first detailed shaded relief maps of the satellite. The shape is approximated by a triaxial ellipsoid with axes of 144, 108 and 98 km. The volume is estimated to be $8 \pm 1 \times 10^5$ km^3. A prominent valley and several grooves are found on the heavily cratered surface.

Introduction

The smaller of the Saturnian co-orbital satellites, Epimetheus was observed by the cameras of Voyagers 1 and 2 in 1980 and 1981 respectively (Smith *et al.*, 1981, 1982). Eight Voyager images were used to create a topographic model and map of Epimetheus. The satellite has approximate dimensions of 144 by 108 by 98 km. The images reveal a major east-west valley on the Saturn-facing side which has not been described before, and several smaller groove-like features. The satellite has several craters larger than 30 km in diameter and numerous craters down to the resolution limit of about 5 km.

This is the third in a series of papers on the topography of non-spherical worlds, following studies of the nucleus of Halley's Comet (Stooke and Abergel, 1991) and the jovian satellite Amalthea (Stooke, 1992a). The other co-orbital satellite, Janus, and Saturn's other small satellites will be the subjects of future reports.

Data

The eight Voyager images of Epimetheus used for this study are listed in Table I. They are identified by FDS (Flight Data Subsystem) number. The first digit of the FDS number is 3 for a Voyager 1 image and 4 for a Voyager 2 image. The Voyager 1 images were taken from Planetary Data System (PDS) CD-ROMs. The Voyager 2 images are not yet available on PDS CD-ROMs and were obtained on tape from NASA's National Space Science Data Center.

Latitudes and longitudes given in this paper are planetocentric. The quoted latitudes assume a rotation axis perpendicular to the orbit plane, and the quoted longitudes assume synchronous rotation. The prime meridian faces Saturn and longitudes increase opposite to the direction of rotation, following planetary cartographic conventions. The rotation assumptions are discussed below with regard to the results of the shape analysis and mapping.

Table I
Voyager images of Epimetheus

| FDS number | Spacecraft | | Sun | | Resolution |
	lat	long	lat	long	(km/line pair)
34942.29*	−45	290	4	316	3.4
34942.33	−45	290	4	317	3.4
34942.37	−45	291	4	319	3.3
34942.41	−46	291	4	320	3.3
34942.45*	−46	292	4	322	3.2
34942.49	−46	293	4	321	3.2
43991.14*	21	91	8	134	12.4
43995.54*	35	185	8	225	6.4

* Images used to model and map Epimetheus.

The six Voyager 1 images (FDS 34942.29 to 34942.49) were taken in one multispectral sequence and show the shadow of Saturn's F Ring crossing the surface of Epimetheus, giving six surface profiles which were incorporated into the topographic model. Two of these images (FDS 34942.29 and 34942.45) give the highest resolution views of the surface, about 1.6 km per pixel. The remaining Voyager 1 images are smeared by varying amounts, though not so badly that the F Ring shadow cannot be traced across the surface. The two sharp images are separated in viewing direction by only 3 degrees, and so do not form an effective stereoscopic pair.

Voyager 2 obtained two images at greater distances which extend imaging coverage to about 80% of the surface. The largest missing area, the south polar region, is in shadow in Voyager 1 images and beyond the limb in the Voyager 2 images. The other area not seen in any images is on the prime meridian between the equator and 60 °N. Image 43991.14 has a resolution of 6.2 km per pixel and shows only larger topographic features, but it provides the only coverage of most of the leading side. Image 43995.54 extends coverage of the northern hemisphere at 3.2 km per pixel, but has only a very slight overlap with the other images, so again no stereoscopic viewing is possible.

Method

The shape of Epimetheus was modelled from limb and terminator positions in the four images identified with an asterisk in Table I, using the methods described by Stooke and Keller (1990), Stooke and Abergel (1991) and Stooke (1992a). Limb and terminator positions were digitized from the images. An initial triaxial ellipsoid model was created using the axis dimensions (140 by 115 by 100 km) given by Thomas *et al.* (1983). This model was viewed and illuminated in the orientations given in Table I and registered to the outlines digitized from the images. The model was iteratively reshaped until it duplicated the appearance of the limbs and terminators in the four useful images. Figure 1 shows the positions of limb and terminator traces on the model. Areas where several traces coincide (e.g., from

EPIMETHEUS
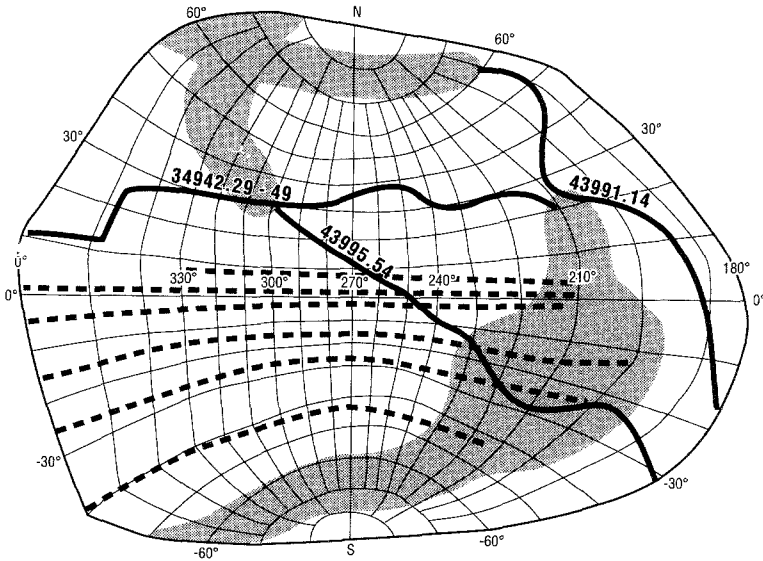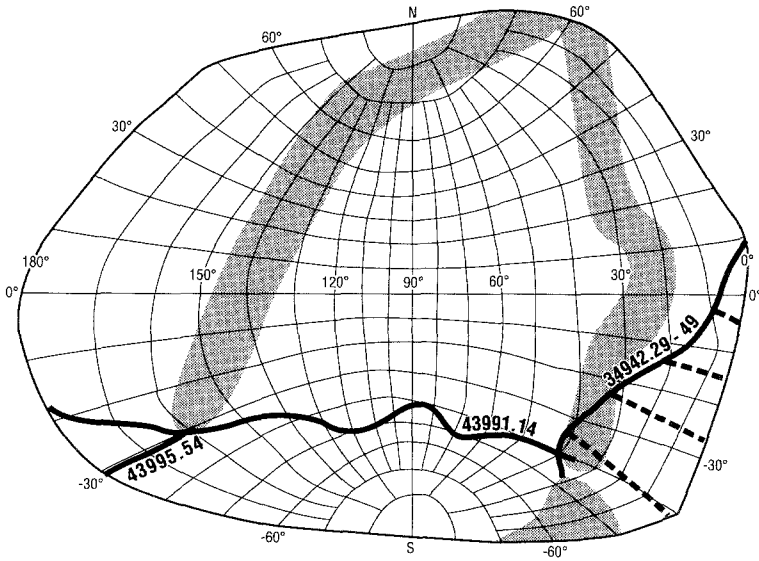
Fig. 1.   Locations on Epimetheus of the sources of shape information: limbs (solid lines), terminators (shaded areas) and ring shadows (dotted lines). The map projection is the same as that used in Figures 4 to 6.

30 °N to 30 °S, 200° to 240 °W) are modelled most reliably, whereas regions not crossed by a limb or terminator are least reliable. Some attempt was made at this stage to model features, particularly ridges and craters, which appear on the images but are not seen on a limb or terminator. Contours in these regions are merely suggestive of the local topography.

The limbs are probably located to within about one pixel in the plane of the image, and the terminators to within about two pixels. Uncertainties are caused by smearing, aliasing effects at the limb, and low signal levels near the terminators. When the limbs are transferred to a body-fixed coordinate system for mapping, their locations may be uncertain by up to several tens of degrees perpendicular to the limb traces of Figure 1, reducing reliability in the model to no better than about two pixels even in the best areas. Relative elevations near terminators may be accurate to within a few hundred meters in places, since small variations in topography produce large changes in the shape of the terminator. Absolute radii near terminators are reasonably reliable only near limb traces, within the limits outlined above. Despite these considerable uncertainties, the model derived by these techniques is the best yet available since the low resolution and minimal overlap between images preclude stereoscopic imaging and control point triangulation.

A unique source of additional topographic data for Epimetheus is the shape of the F Ring shadow in six Voyager 1 images. After modelling based on limbs and terminators was complete, the ring shadows were digitized from the images and registered with the model in the Voyager 1 orientation. The shadows were projected onto the model as seen from the sun direction. The portion of the ring whose shadow fell across the disk of Epimetheus was assumed to be perfectly linear. Given the kinks and braids observed in some sections of the F Ring (Smith *et al.*, 1981, 1982) this may not be precisely correct, but since the true shape of the ring at the location casting the shadow is unknown the simplest assumption was made. The topographic model was modified to remove any deviations from a straight line in the shadows as seen from the sun direction. The approximate positions of the sometimes ill-defined ring shadows are shown as dashed lines in Figure 1. It is hard to quantify the reliability of modelling based on ring shadows, but it should considerably enhance the representation of the region centred on 20 °S, 330 °W, which would otherwise be very poorly constrained. It is apparent from Figure 1 that the shape of the trailing side of Epimetheus (centred on longitude 270°) is very much more reliably known than is the shape of the leading side.

The Shape of Epimetheus

The topographic model is presented in Table II and illustrated in Figures 2 to 7. The original data for Table II, at the 5° spacing used during modelling is available from the author on diskette. Latitude-longitude grids corresponding to three Voy-

Voyager 1   34942.29-49   Voyager 2   43991.14
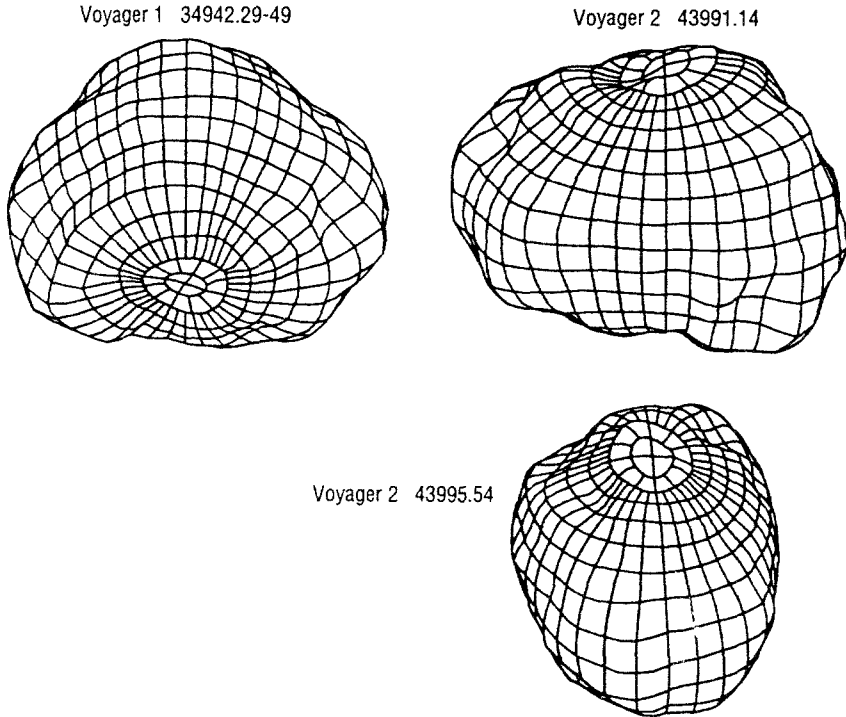
Voyager 2   43995.54

Fig. 2.   Latitude-longitude grids in orthographic projection corresponding to three Voyager images. See Table I for further details. The remaining Voyager 1 images listed in Table I are almost identical to image 34942.29.

ager views are given in Figure 2. The rotation axes are vertical in these views regardless of the actual orientation of the satellite in the images. Six mutually perpendicular views are presented in Figure 3, including polar views which show the estimated shape of the equator.

Figure 4 is a shaded relief map of the surface of Epimetheus on a Morphographic Conformal projection, which is a conventional Stereographic projection modified for use with non-spherical objects (Stooke, 1986). The shape which has been used to control the projection is the three dimensional convex hull of the Epimetheus topographic model, a refinement of this mapping procedure designed to reduce distortion (Stooke, 1992b) and used here for the first time. The outline of each map is the convex hull of the satellite in the plane containing the long and short (rotation) axes. Only two craters on Epimetheus have been given names by the International Astronomical Union (1983). They are identified in Figure 4.

In Figure 5 the shaded relief drawing has radius contours superimposed. Radii are given in kilometres with a contour interval of 5 km. Elevations relative to the original 140 by 115 by 100 km triaxial ellipsoid are superimposed on relief in Figure 6. The radius and elevation contours are also plotted on the simple cylindrical projection in Figure 7.

Table II
Radius matrix for the Epimetheus model (km)

Latitude	Longitude									
	90	80	70	60	50	40	30	20	10	0
90	49.5	49.5	49.5	49.5	49.5	49.5	49.5	49.5	49.5	49.5
80	49.2	49.4	49.5	49.7	49.8	50.0	50.6	51.1	51.6	52.4
70	47.1	47.8	49.1	50.3	50.7	51.8	52.9	53.8	55.0	55.9
60	48.1	48.9	50.0	51.3	52.1	54.1	56.0	57.8	58.6	59.1
50	48.6	49.6	51.1	52.4	51.2	54.2	58.7	60.1	59.2	58.8
40	50.0	51.3	53.0	54.5	54.7	58.2	63.7	63.4	58.8	57.5
30	51.4	51.1	52.8	56.5	60.0	64.2	66.6	65.5	58.4	54.8
20	52.1	52.6	55.6	58.2	61.9	62.9	66.8	64.8	59.2	54.7
10	51.3	50.5	55.2	59.0	60.8	60.9	66.8	66.9	64.1	62.9
0	52.0	52.7	56.3	59.5	61.9	63.4	67.9	67.4	65.6	61.1
−10	49.8	51.3	57.1	61.5	62.6	66.7	67.9	69.7	69.3	60.6
−20	51.9	53.8	60.4	57.5	60.4	69.4	70.9	67.9	64.4	60.3
−30	52.2	54.6	59.3	58.6	62.8	72.9	72.5	67.3	63.0	59.5
−40	53.3	54.3	60.9	63.4	66.5	69.7	71.1	68.3	66.2	64.6
−50	49.8	49.2	54.1	55.9	57.2	58.5	59.8	61.7	59.7	57.8
−60	46.8	46.2	46.5	47.4	48.4	49.3	49.5	50.0	51.8	53.9
−70	44.7	44.2	44.6	44.8	45.1	45.4	46.0	46.8	48.2	49.7
−80	42.9	42.8	42.8	42.9	43.1	43.4	43.8	44.2	44.7	45.2
−90	44.0	44.0	44.0	44.0	44.0	44.0	44.0	44.0	44.0	44.0

Latitude	Longitude									
	180	170	160	150	140	130	120	110	100	90
90	49.5	49.5	49.5	49.5	49.5	49.5	49.5	49.5	49.5	49.5
80	45.5	45.5	45.7	46.2	46.7	47.4	48.2	49.0	49.1	49.2
70	46.0	46.0	46.5	46.9	47.5	48.2	48.0	47.4	47.1	47.1
60	52.0	50.8	50.5	49.5	48.5	47.4	46.9	47.0	47.7	48.1
50	56.6	52.8	51.9	51.3	48.8	47.4	47.7	48.2	48.1	48.6
40	58.0	53.9	51.1	50.7	49.7	48.3	48.6	49.7	49.5	50.0
30	60.0	57.1	53.7	53.5	53.7	51.4	51.6	51.2	50.7	51.4
20	59.7	61.2	59.4	59.3	59.3	55.0	53.0	52.0	51.5	52.1
10	68.0	66.5	65.1	66.3	65.4	58.9	54.2	52.2	51.7	51.3
0	72.7	70.3	68.6	68.4	66.5	61.0	54.9	52.4	51.8	52.0
−10	72.9	70.8	70.6	69.0	64.0	59.7	54.3	52.3	51.8	49.8
−20	70.3	70.9	71.1	67.2	61.9	57.0	53.4	52.1	51.7	51.9
−30	66.7	67.8	66.1	62.6	59.4	57.4	54.3	52.7	51.7	52.2
−40	59.8	60.4	57.6	54.7	54.6	55.8	54.6	53.1	51.8	53.3
−50	54.4	54.7	54.2	53.1	52.4	52.5	51.9	51.2	49.6	49.8
−60	50.5	51.6	52.3	52.1	51.4	50.7	49.8	48.7	47.5	46.8
−70	47.2	47.4	47.8	47.7	47.7	47.4	46.7	46.0	45.2	44.7
−80	45.8	45.4	45.0	44.7	44.4	44.1	43.7	43.4	43.1	42.9
−90	44.0	44.0	44.0	44.0	44.0	44.0	44.0	44.0	44.0	44.0

Epimetheus is very irregular in shape, as clearly seen in Figures 2 and 3. The equatorial outline is roughly elliptical with prominent ridges near longitudes 30°, 140° and 195°. Equatorial views centred at longitudes 90° and 270° indicate a tapered body, considerably broader from north to south on the side facing Saturn. The south polar region, which is nowhere observed in the images, appears to be

Table II.   Continued

Latitude	Longitude									
	270	260	250	240	230	220	210	200	190	180
90	49.5	49.5	49.5	49.5	49.5	49.5	49.5	49.5	49.5	49.5
80	50.6	50.1	49.8	49.0	48.1	47.3	46.6	46.0	45.7	45.5
70	51.1	50.9	50.0	49.4	49.7	49.3	48.1	47.1	46.3	46.0
60	51.5	50.9	48.3	47.2	48.1	50.4	51.5	52.3	52.5	52.0
50	53.9	53.6	52.0	50.0	50.3	51.7	54.8	57.3	58.5	56.6
40	57.2	58.0	58.5	57.9	57.1	57.4	55.8	57.9	60.2	58.0
30	57.8	57.1	57.8	58.8	59.1	61.8	63.4	61.1	61.5	60.0
20	56.7	57.2	57.7	59.2	59.5	64.6	69.9	70.9	65.7	59.7
10	58.2	59.5	57.8	59.0	60.0	65.6	73.0	75.9	76.8	68.0
0	55.7	54.6	56.1	57.9	62.7	67.7	73.0	76.4	78.4	72.7
−10	53.6	53.4	54.0	57.3	62.9	66.0	70.7	77.5	78.7	72.9
−20	49.4	50.4	52.0	55.2	59.9	58.2	61.9	69.5	73.2	70.3
−30	47.1	46.5	47.1	52.8	58.0	60.1	61.5	63.7	65.7	66.7
−40	46.3	45.5	45.4	47.2	51.7	56.6	58.1	56.9	58.9	59.8
−50	46.0	45.1	45.0	45.8	48.2	55.2	55.6	54.4	54.5	54.4
−60	49.3	46.3	45.5	46.0	49.0	52.6	50.9	50.2	50.2	50.5
−70	51.6	51.4	51.2	50.4	48.7	47.0	47.0	46.8	46.7	47.2
−80	48.2	48.2	48.2	48.1	48.0	47.6	47.1	46.7	46.2	45.8
−90	44.0	44.0	44.0	44.0	44.0	44.0	44.0	44.0	44.0	44.0

Latitude	Longitude									
	360	350	340	330	320	310	300	290	280	270
90	49.5	49.5	49.5	49.5	49.5	49.5	49.5	49.5	49.5	49.5
80	52.4	53.0	53.4	53.5	53.4	53.0	52.3	51.6	51.0	50.6
70	55.9	56.8	57.1	56.7	55.6	54.0	52.9	52.1	51.3	51.1
60	59.1	58.9	57.8	54.7	54.7	52.4	51.8	51.5	51.3	51.5
50	58.8	59.4	59.8	57.4	55.1	52.3	51.4	52.4	53.1	53.9
40	57.5	57.6	56.5	55.6	54.2	53.2	52.8	53.6	55.8	57.2
30	54.8	54.0	53.8	55.0	57.9	57.5	60.5	60.5	59.1	57.8
20	54.7	55.6	54.3	54.0	55.3	56.6	58.0	58.7	58.6	56.7
10	62.9	59.3	57.0	56.1	55.0	55.9	57.1	58.3	58.0	58.2
0	61.1	57.8	55.5	54.0	53.8	53.6	52.8	53.2	54.2	55.7
−10	60.6	57.6	54.2	54.0	53.9	55.5	53.2	52.8	52.9	53.6
−20	60.3	57.7	52.3	51.4	50.8	50.7	51.6	50.6	50.8	49.4
−30	59.5	57.6	55.0	53.8	53.6	53.7	54.9	51.5	50.0	47.1
−40	64.6	64.8	62.9	61.0	61.3	59.6	57.9	56.1	49.6	46.3
−50	57.8	58.4	58.2	57.9	57.3	56.7	56.0	55.2	50.7	46.0
−60	53.9	55.0	55.2	55.1	54.8	54.4	54.0	53.6	52.5	49.3
−70	49.7	50.6	51.4	52.1	52.6	52.5	52.3	52.0	51.8	51.6
−80	45.2	45.7	46.1	46.6	47.0	47.4	47.7	47.9	48.1	48.2
−90	44.0	44.0	44.0	44.0	44.0	44.0	44.0	44.0	44.0	44.0

considerably flattened. The flattening is probably caused by the presence of at least one large crater near the south pole. The view from the planet (centred on longitude 0°) is irregular but fairly symmetrical.

The maximum radius in the model is 79.1 km at 5 °N, 190 °W. The minimum radius is 42.8 km at 80 °S, 75 °W, though it must be remembered that in this region the radii are very weakly constrained. The equatorial diameter of the model from

lat 0° long 0°   lat 0° long 180°

lat 0° long 90°   lat 0° long 270°
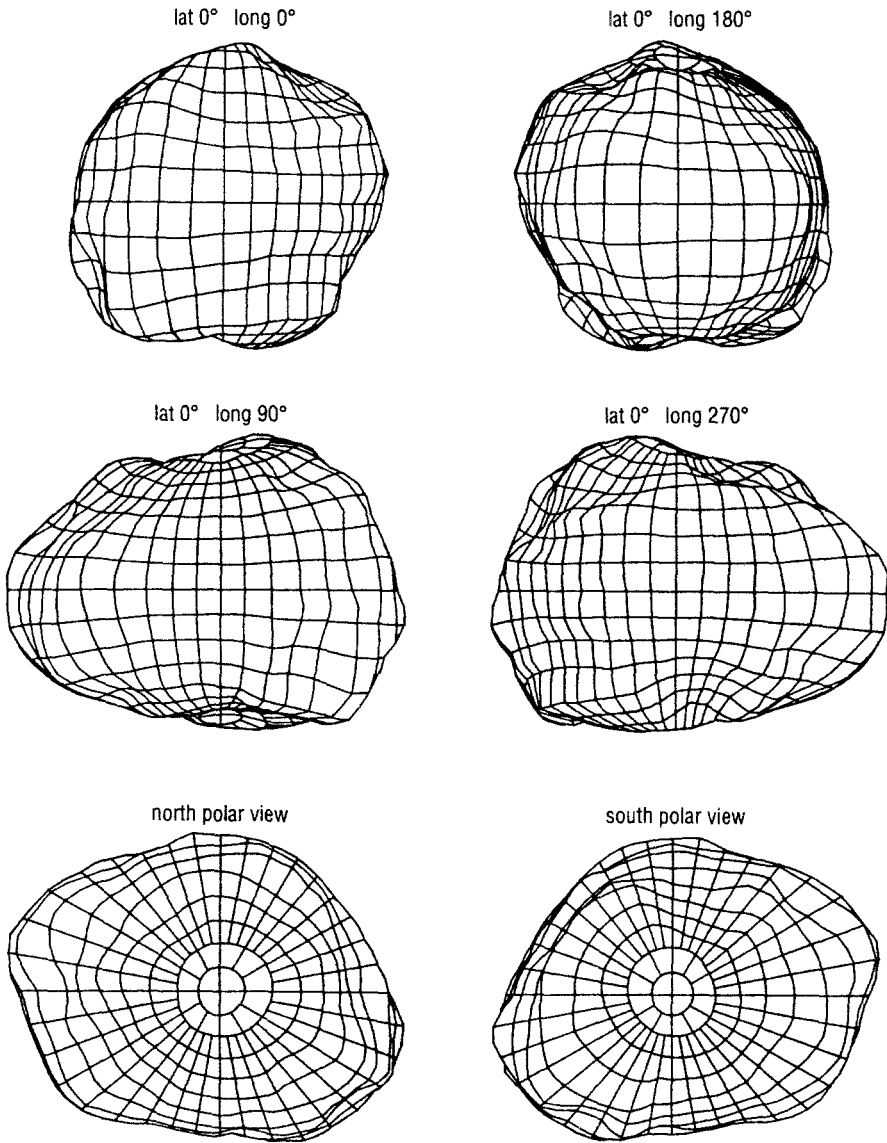
north polar view   south polar view

Fig. 3.   Orthographic latitude-longitude grids representing Epimetheus, viewed from six mutually perpendicular directions.

0° to 180° longitude is 133.7 km. From 90° to 270° the equatorial diameter is 107.7 km, and the polar diameter of the model is 93.5 km. The maximum equatorial dimension is slightly offset from the Saturn-facing meridian, being 144 km from 10° to 190° longitude. The offset may be weak evidence of a libration, but the radii near 190° are based on the limb in the lowest resolution image used for this study and are uncertain by 10 to 15 km.

EPIMETHEUS
shaded relief

Cartographic Section
Department of Geography
University of Western Ontario

0   20 km   0   20 km
centre of map   edge of map

morphographic conformal
projection
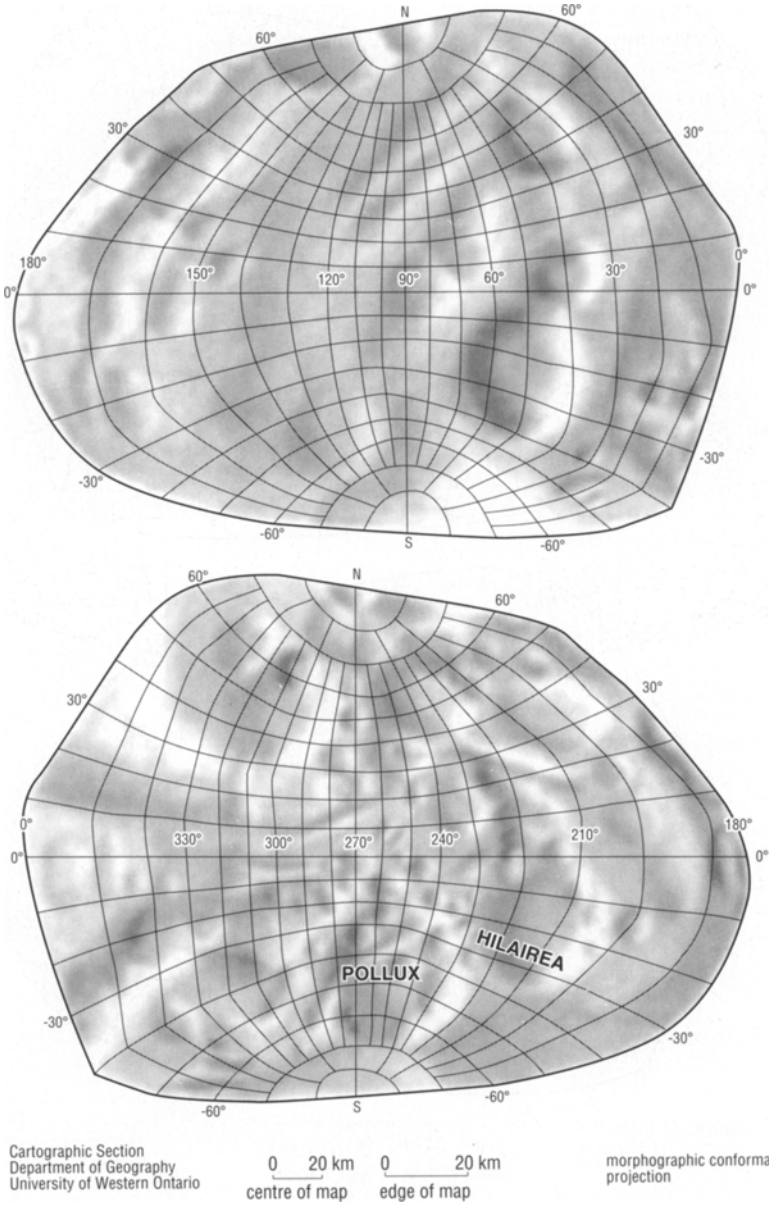
Fig. 4.   Shaded relief map of Epimetheus on the Morphographic Conformal Projection.

EPIMETHEUS
shaded relief and radii
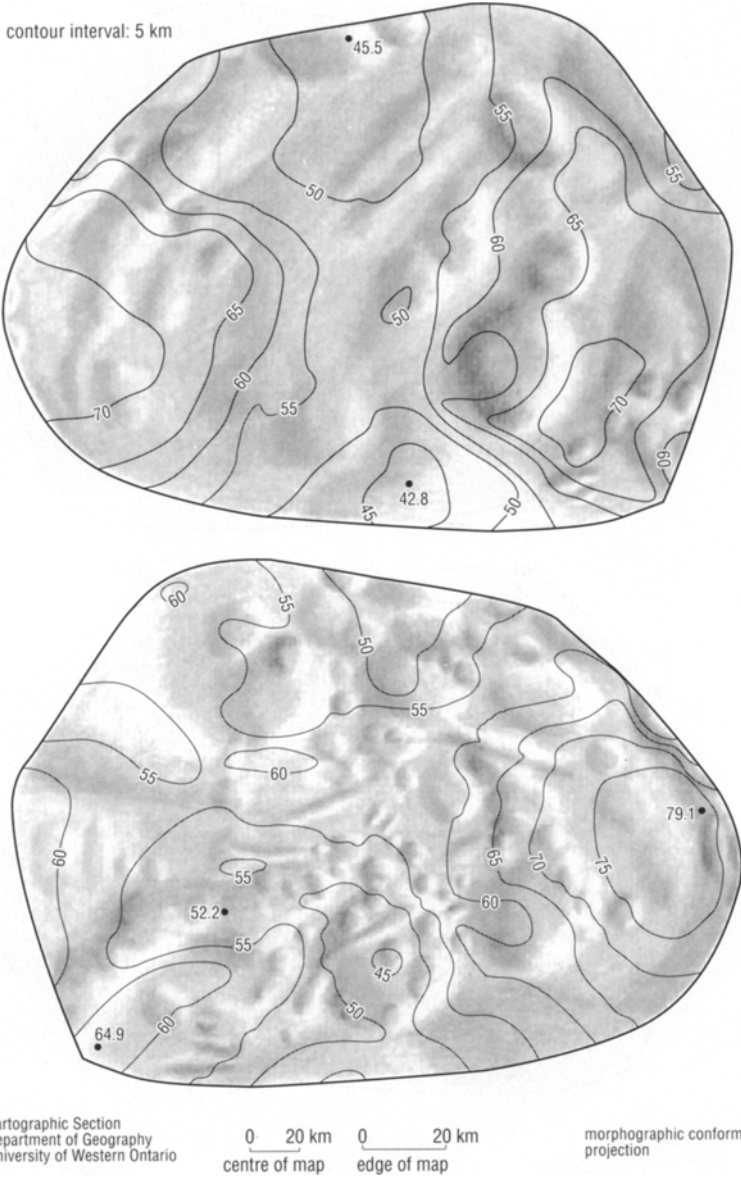
Fig. 5.   Shaded relief map of Epimetheus with contours of local radius in kilometres at 5 km intervals.

EPIMETHEUS
shaded relief and elevations

datum: 140 x 115 x 100 km ellipsoid
contour interval: 5 km
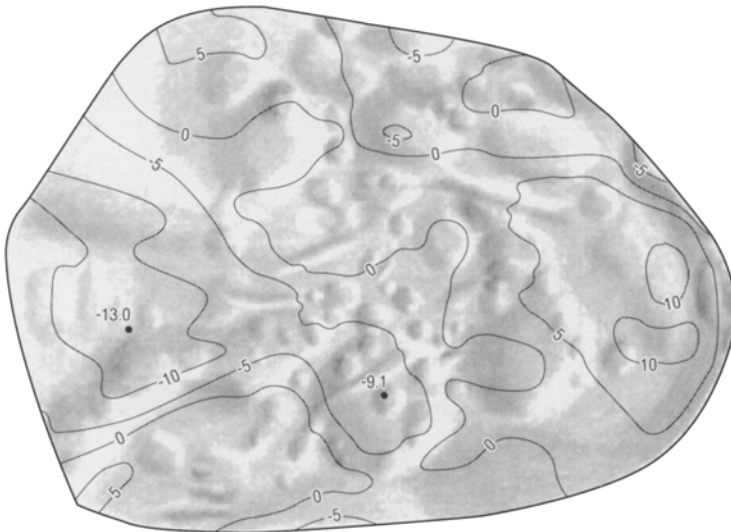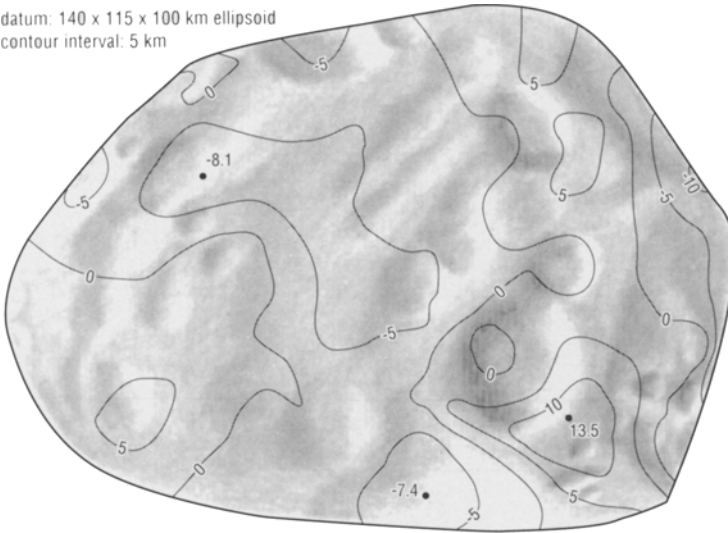
Cartographic Section
Department of Geography
University of Western Ontario

0   20 km   0   20 km
centre of map   edge of map

morphographic conformal
projection

Fig. 6.   Shaded relief map of Epimetheus with contours of elevation relative to a 140 by 115 by 100 km
triaxial ellipsoid. The contour interval is 5 km.

RADII
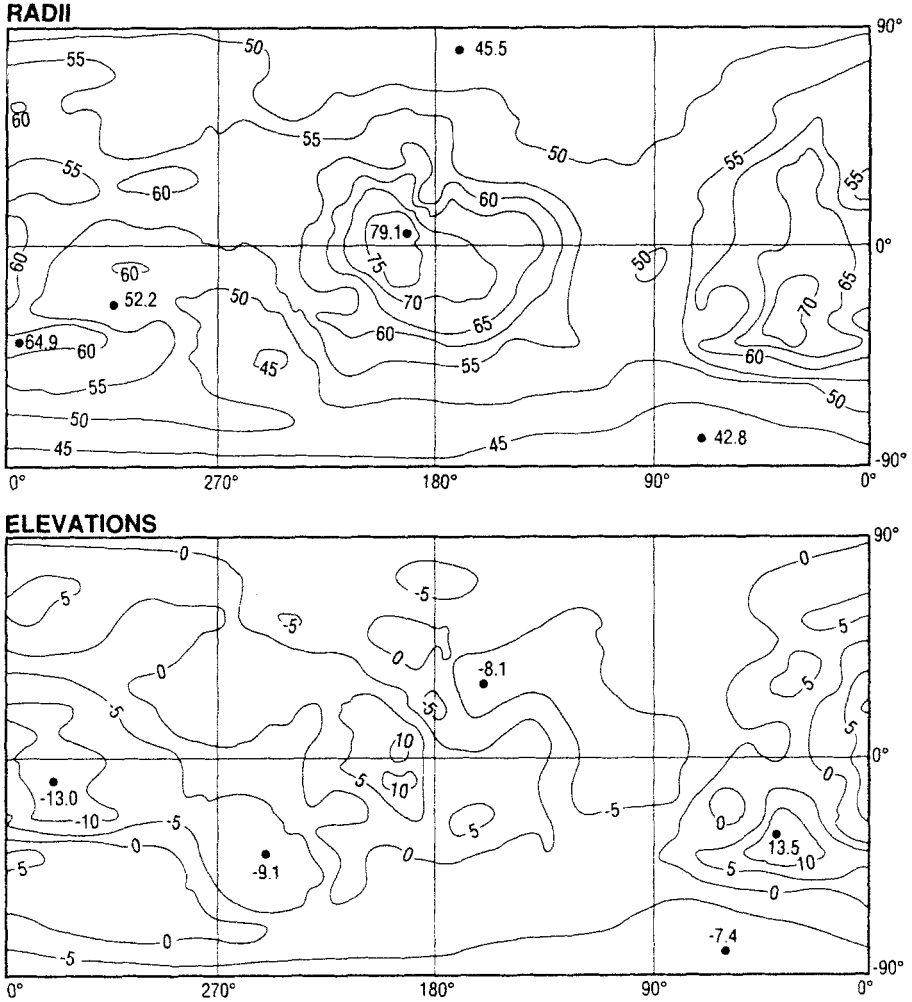
ELEVATIONS

Fig. 7.   Radius and elevation contours from Figures 5 and 6 on a simple cylindrical projection.

The volume of the model is $8.0 \pm 1.0 \times 10^5 \, \text{km}^3$. This is slightly lower than the previous estimate of $8.8 \pm 1.4 \times 10^5 \, \text{km}^3$ by Thomas (1989), based on a best fit triaxial ellipsoid and using essentially the same uncertainty in radius assumed here (about ± 2.5 km). The triaxial ellipsoid used by Thomas (1989) has dimensions of 138, 110 and 110 km, already smaller than the earlier ellipsoidal model (Thomas *et al.*, 1983) adopted as the starting point for this analysis. This analysis suggests that a triaxial ellipsoid with axes of 144, 108 and 98 km gives a better estimate of volume. Yoder *et al.* (1989) estimated the mean density of Epimetheus as $0.64 \pm 0.12 \, \text{g/cm}^3$, "smaller than any other satellite density in the solar system". The slightly smaller volume suggested here gives a density of about $0.7 \, \text{g/cm}^3$, still

unusually low and suggesting significant porosity, though less than is required with the density suggested by Yoder *et al.* (1989).

A preliminary map and model of Epimetheus was presented by Stooke (1988) and Stooke and Keller (1990), primarily to illustrate the class of map projections used in Figures 4, 5 and 6. They differ considerably from the results presented here. The differences result from the use here of digital rather than hard-copy images, the use of the low resolution image 43991.14 in this study but not the earlier work, better registration of images with the model and the inclusion of terminator data. The preliminary model was based only on limb shapes. Thus the preliminary model is wholly superseded by that presented here.

Rotation

Epimetheus was assumed to be in synchronous rotation with a period of 16.66 hr (Smith *et al.*, 1982) and negligible librations. Substantial librations, or even chaotic rotation, might be anticipated because of the frequent gravitational interactions between the co-orbital satellites. Given the very limited number of useful images, it is not possible to support or refute these assumptions. There is no useful overlap between illuminated areas in the three imaging sequences, so no single small feature can be recognised in more than one view. The only area of overlap is north of the equator around longitude 160°. Several craters are visible here in image 43995.54, but the same area in image 43991.14 is seen obliquely at very low resolution and near the sub-solar point. Even extreme contrast enhancement is unable to reveal any certain features. However, the following points may be made regarding the rotation of Epimetheus:

First, if the rotation was very much faster than synchronous the Voyager 1 image sequence would show the effects of rotation. The two sharpest images in that sequence (34942.29 and 34942.45) were taken 13 min apart, corresponding to about 4.7° of rotation. The motion of the spacecraft reduces that to about 3° of apparent rotation, barely detectable in images of this resolution. The most rigorous constraint on rotation is probably the position of the shadow cast by the western rim of the crater Hilairea (Figure 4) on its eastern floor and rim in the two sharpest images. The change in position is consistent with synchronous rotation. A rotation period of less than about 12 h can certainly be ruled out.

Second, a very long period can be excluded by the changes between the two Voyager 2 images. Rotation carried all recognizable features in image 43991.14 off the disk before image 43995.54 was obtained. Any period longer than about 24 h would leave much of the leading side of Epimetheus visible in the second image. The orientations of the long and short axes in all the images are consistent with the expected synchronous rotation.

Third, a weak constraint on rotation is given by the failure of distinctive features to recur in different views. The craters Pollux and Hilairea and the large valley

and ridge in the Voyager 1 images would be visible even in the lowest resolution Voyager 2 image if an unexpected rotation state had carried them into view.

The rotation state should be fairly easy to confirm given even a few more images from the Cassini spacecraft at resolutions of 2 km/pixel or better. Repetitive imaging at resolutions exceeding 1 km/pixel could be used to search for librations caused by interactions with Janus.

Surface Features

The shaded relief drawing shows craters in all areas imaged at sufficient resolution. The largest are Pollux and Hilairea, each about 40 km across. Both of the areas which do not appear in any images (the south pole and the region around 30 °N on the prime meridian) are probably not seen because they are depressed, and so may contain large craters. The position and shape of the terminator in the Voyager 1 images is certainly suggestive of a large crater rim. There are about ten certain craters with diameters in the 25 to 40 km range, and several other possible craters suggested by depressions in the limbs and terminators. The less certain craters are drawn less distinctly on the maps. Where the resolution is sufficient to resolve craters of 5 to 10 km they appear in profusion. No areas are clearly observed to lack craters.

Small irregular depressions may easily be confused with impact craters near the limit of resolution, a tendency which is probably exaggerated in the shaded relief drawing, so interpretations must be undertaken with caution. For this reason the crater counts given by Plescia and Boyce (1982, 1983) and Thomas *et al.* (1983) will not be updated here even though the present map appears to show more craters than were included in those counts.

Thomas *et al.* (1983) state that one region of Epimetheus, from 290° to 340 °W and 0° to 40 °S "appears bland and may be relatively smoother than the rest of the satellite's surface". This area is near the sub-solar point in Voyager 1 images. Features including faint apparent craters and a large valley (described below) are mapped in the region in Figure 4. The bland appearance disappears with extreme contrast enhancement, suggesting that the statement of Thomas *et al.* is probably not correct. Plescia and Boyce (1983) suggest that one region (presumably the same area described as bland by Thomas *et al.*) "has distinctly lower crater numbers which may represent the event during which [Janus and Epimetheus] were split apart". The present study does not support that statement.

The existence of pervasive cratering over all parts of Epimetheus observed at sufficient resolution suggests that the surface must be several billion years old. If the co-orbital satellites formed by disruption of a single parent body, the impact occurred relatively early in the history of the satellite system. This is consistent with the appearance of the other co-orbital satellite, Janus, which is also heavily cratered. Preliminary work on a model and map of Prometheus, the inner F Ring shepherd satellite, suggests fewer craters at comparable image resolutions and a

younger surface. Pandora, the outer F Ring shepherd, is poorly imaged but appears to have an older, heavily cratered surface. Thus the inner satellites of Saturn may have diverse surface ages and histories, but Epimetheus in particular must be old.

One of the most prominent topographic features revealed in the Voyager images is a large groove or valley extending about 100 km from 20 °S, 280 °W to 30 °S, 30 °W across the Saturn-facing side of the satellite. It is roughly 12 km wide through most of its length, widening at the eastern end to nearly 20 km across before becoming lost in a rugged cratered area. The apparent widening of the valley towards the prime meridian in Figure 4 is caused by the increase in scale towards the perimeter of the map in this conformal projection. In fact the sides of the valley are roughly parallel except near the eastern end. The valley is not seen near the terminator so there are no cast shadows to indicate its depth. The F Ring shadows are nearly parallel with the valley and so unfortunately do not give a topographic profile. A depth of several kilometers is indicated in Figure 5, but this is merely suggestive and is not usefully constrained in any way.

A long straight ridge forms part of the limb at 10 °N, 350 °W. It appears to extend some 50 km to the east where it apparently forms the southern edge of a valley similar in scale to that described above. This possible valley is poorly seen and may consist of overlapping craters, but the straight ridge is reasonably certain. It is shown on an unpublished map by Peter C. Thomas (personal communication to the author), along with several of the lesser grooves described below. The large valley described above is only revealed by extreme contrast enhancement and has not been described previously.

Several short groove segments are visible in the highest resolution frames, typically about 5 km wide and up to 40 km long (Figure 8). Most are oriented roughly east-west, parallel with the large valley. These grooves are near the limit of resolution even in the best images, and some might consist of chance alignments of small craters or other topographic features. The lower resolution Voyager 2 frames also show linear topographic features. Two parallel valleys or crater chains trending northeast to southwest are seen at 50 °N, 90 °W in the lowest resolution image (FDS 43991.14). Their widths are near the limit of resolution, about 10 to 15 km. Between longitudes 150° and 200° in image 43995.54 are several vague north-south linear features, probably chance alignments of large crater rims for the most part. One feature appears more significant and is mapped as a prominent groove at 30 °N, 220 °W. The grooves near the equator and longitude 290° are seen only as linear bright or dark markings at very high sun angles. The interpretation as grooves may be suspect.

These linear features suggest fairly large scale disruption of the satellite. Endogenetic tectonism is presumably lacking in such a small body, so the most likely causes of disruption are fracturing during catastrophic disruption of a parent body or pervasive fracturing of the satellite associated with the formation of a large crater. Many smaller bodies appear to have been heavily fractured by large impacts, notably Phobos (Thomas, 1979) and Mimas (Stooke, 1989). Since the
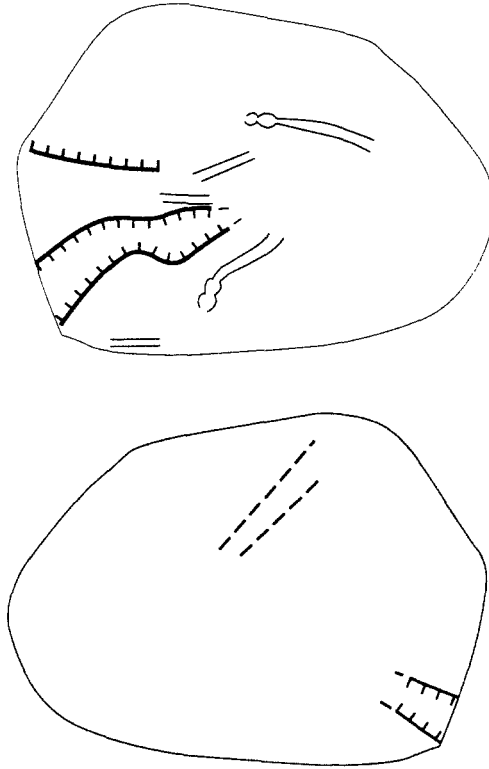
Fig. 8. Sketch of major non-crater features on Epimetheus: scarps (single lines, ticks downslope), grooves (double lines, scalloped where the groove resembles a crater chain) and possible valleys, poorly resolved (dashed lines).

surface of Epimetheus is heavily cratered and grooves appear to cut craters in several places (e.g., 50 °S, 270 °W; 30 °N, 220 °W), I interpret the grooves as being caused by a relatively recent large impact rather than dating to the formation of Epimetheus by fragmentation from a parent body. The large valley may share that origin, but as suggested in Figure 4 there may be a substantial number of superimposed craters so an older date seems more likely. It and the other very large linear features may have formed during the disruption of the co-orbital satellites' parent body.

Fractures on Phobos appear from their global distribution to have been caused by the impact which formed Stickney, the largest crater on the satellite (Thomas, 1979). The grooves on Mimas may have a similar relationship to the crater Herschel (Stooke, 1989). If the few grooves present on Epimetheus have a similar origin, global high-resolution coverage might permit identification of the associated crater. Existing coverage at sufficient resolution is too limited to identify the crater today. A good candidate would be the large deep crater at 20 °S, 50 °W, near the western end of the large valley. During the Cassini mission it should be possible to obtain images at least as good as the best from Voyager 1 for a number of

viewing and illumination conditions. With such images the global groove distribution could be observed and the topographic model of Epimetheus would be substantially improved.

Acknowledgements

References

International Astronomical Union (IAU):, 1983, *Trans.* Vol. XIXB, D. Reidel, Dordrecht, pp. 331–345.

Plescia, J. B. and Boyce, J. M.: 1982, *Nature* **295**, 285–290.

Plescia, J. B. and Boyce, J. M.: 1983, *Nature* **301**, 666–670.

Smith, B. A., Soderblom, L., Beebe, R., Boyce, J., Briggs, G., Bunker, A., Collins, S. A., Hansen, C. J., Johnson, T. V., Mitchell, J. L., Terrile, R. J., Carr, M., Cook, A. F., Cuzzi, J., Pollack, J. B., Danielson, G. E., Ingersoll, A., Davies, M. E., Hunt, G. E., Masursky, H., Shoemaker, E., Morrison, D., Owen, T., Sagan, C., Veverka, J., Strom, R. and Suomi, V. E.: 1981, *Science* **212**, 163–191.

Smith, B. A., Soderblom, L., Batson, R. M., Bridges, P., Inge, J., Masursky, H., Shoemaker, E., Beebe, R., Boyce, J., Briggs, G., Bunker, A., Collins, S. A., Hansen, C. J., Johnson, T. V., Mitchell, J. L., Terrile, R. J., Cook, A. F., Cuzzi, J., Pollack, J. B., Danielson, G. E., Ingersoll, A. P., Davies, M. E., Hunt, G., Morrison, D., Owen, T., Sagan, C., Veverka, J., Strom, R. and Suomi, V. E.: 1982, *Science* **215**, 504–537.

Stooke, P. J.: 1986, Proceedings 2nd International Symposium Spatial Data Handling, Seattle, July, 1986, pp. 523–536.

Stooke, P. J.: 1988, PhD dissertation, University of Victoria, 169 pp.

Stooke, P. J.: 1989, *Lunar Planet. Sci.* **XX**, Houston, Texas, pp. 1069–1070.

Stooke, P. J.: 1992a, *Earth, Moon, and Planets* **56**, 123–139.

Stooke, P. J.: 1992b, Proceedings, Asteroids, Comets, Meteorites, 1992.

Stooke, P. J. and Abergel, A.: 1991, *Astron. Astrophys* **248**, 656–688.

Stooke, P. J. and Keller, C. P.: 1990, *Cartographica* **27**, 82–100.

Thomas, P.: 1979, *Icarus* **40**, 223–243.

Thomas, P. C.: 1989, *Icarus* **77**, 248–274.

Thomas, P., Veverka, J., Morrison, D., Davies M. and Johnson, T. V.: 1983, *Journ. Geophys. Res.* **88**, 8743–8754.

Yoder, C. F., Synnott, S. P. and Salo H: 1989, *Astron. Journ.* **98**, 1875–1889.